

Periodic switching in a recombinase-based molecular circuit

Christian Cuba Samaniego¹, Giulia Giordano² and Elisa Franco³

Abstract—An important challenge in synthetic biology is the construction of periodic circuits with tunable and predictable period. We propose a general architecture, based on the use of recombinase proteins and negative feedback, to build a molecular device for periodic switching between two distinct regimes; the switching rule depends on known concentration thresholds for some circuit components. We analytically characterise the threshold values for which a periodic orbit is guaranteed to exist and attract all trajectories with initial conditions within an invariant set, and we provide expressions for period and amplitude. We describe two distinct biological realisations of the recombinase architecture, and show their capacity to exhibit periodic behaviours via extensive numerical simulations.

Index Terms—Biomolecular systems, Systems biology

I. INTRODUCTION

DNA recombinases have recently enriched the repertoire of parts in synthetic biology [1]. These enzymes cleave and rejoin DNA strands with high specificity for given domains. By carefully placing these domains, recombinases can perform diverse operations such as DNA excision, insertion, and translocation to generate logic and regulatory circuits [1], [2], [3], [4], [5]. However, it remains an open question whether recombinases can be used to build dynamic systems such as oscillators. Because they introduce a nearly *digital* switch of gene expression (on-off) by reorienting a promoter, the effect of recombinases can be compared to that of transistors in electronic circuits. For this reason, we propose to build recombinase oscillators by taking inspiration from the architecture of *electronic* clocks like astable multivibrators [6]. In contrast, the majority of existing artificial genetic oscillators are regulated via transcription factors, which introduce smooth changes of gene expression, and were developed following classical *analog* circuit design principles, typically by building a negative feedback loop that is destabilised via steep nonlinearities, positive feedback, or delays [7], [8], [9].

First, we describe an *autonomous reset* motif, in which a recombinase reorients a target promoter site and activates expression of a component that causes a reduction of recombinase concentration. Second, by interconnecting two (stable) reset modules, we obtain periodic switching (*set-reset*) when the recombinases exceed a given threshold; switching between two stable modes can generate non-stable dynamics [10], [11],

Work supported by the National Science Foundation through grant CMMI-1266402 to EF, and by the Delft Technology Fellowship grant to GG. Also, CCS acknowledges support from Carlo Maley (ASU) and Ron Weiss (MIT).

¹Biodesign Center for Biocomputing, Security & Society at Arizona State University (ASU), USA, and Department of Biological Engineering at Massachusetts Institute of Technology (MIT), USA. ccubasam@mit.edu

²Delft Center for Systems and Control (DCSC), Delft University of Technology, The Netherlands. g.giordano@tudelft.nl

³Department of Mechanical and Aerospace Engineering, University of California Los Angeles (UCLA), USA. efranco@seas.ucla.edu

[12]. A single recombinase copy is needed to control the orientation of a DNA site, so an advantage of a recombinase oscillator is that its signal may be propagated to other circuits with minimal retroactivity [13].

Relying on classical results on nonlinear systems [14] and on singular perturbation theory [13], [15], we provide an analytical characterisation of the threshold values for which a periodic orbit is guaranteed to exist and we show that, if the thresholds are chosen appropriately, all trajectories starting from suitable initial conditions converge to such a periodic orbit. As previously done in [16] for a relaxation oscillator, we also give analytic expressions for the period and the amplitude of the resulting periodic signal, which can be tuned by altering the production and degradation rates, as well as the thresholds.

Finally, we examine models for two alternative biological implementations of the set-reset circuit: numerical simulations show that both exhibit a periodic behaviour as expected; the dynamics of the systems resemble those of relaxation oscillators [8], [9], [16]. The implementations differ in the biological mechanism chosen to down-regulate the concentration of recombinase (thus “stabilising” each reset module). The fact that alternative mechanisms can be employed without losing the ability to achieve periodic switching suggests that our motif is robust with respect to the chosen realisation.

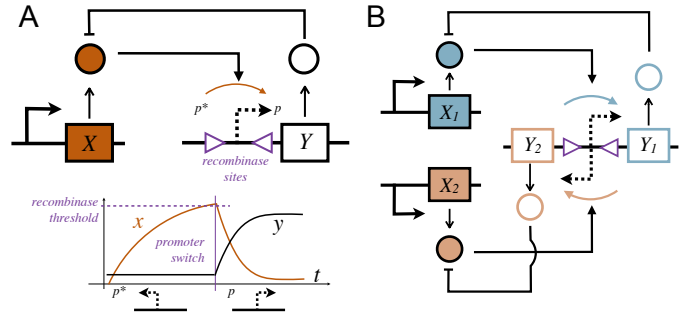


Fig. 1. **Molecular motifs for recombinase-based switching.** A: The reset motif and its qualitative dynamics. B: The set-reset motif resulting from the combination of two reset modules.

II. A BIOMOLECULAR SET-RESET NETWORK

We introduce a recombinase-based network that sets and reset gene expression. We characterise the motif qualitatively; possible specific realisations are discussed in Section IV. We indicate molecular species with uppercase letters, and their concentrations with the corresponding lowercase letters.

An autonomous reset motif. Our motif includes two proteins, X and Y , shown in Fig. 1A. X is a recombinase and its recognition sites are marked by purple triangles. Y is a regulator that causes a reduction in the concentration of X . Initially, Y is not expressed because its promoter site is oriented to the left (p^*), so the amount of X can rapidly

increase (Fig. 1A, bottom). As the recombinase X exceeds a given threshold concentration κ_x , it causes the promoter to flip its orientation (p), which can be viewed as an autonomous *reset* in the circuit. By reorienting the promoter, X switches on the expression of protein Y . As Y increases, it causes a decrease in the concentration of X (negative loop). At this point, the circuit remains in the current state because the concentration of X cannot be increased again. Note that the reorientation of the promoter alters the sequence of the recombinase binding sites, which are no longer available. This system can be modelled by the qualitative ODEs:

$$\dot{x} = b - f(x, y), \quad \dot{y} = \gamma\sigma(x) - \delta y,$$

where $b > 0$ is a constant production rate; f models conversion, dilution, or degradation, and we assume it is an increasing function of both x and y , which is zero when $x = 0$ and tends to infinity when $x \rightarrow \infty$ (hence the existence of an equilibrium point is ensured); $\gamma, \delta > 0$; and $\sigma(x) = 1$ if x exceeds a given threshold, $x \geq \kappa_x$, otherwise $\sigma(x) = 0$. In both configurations, the system is monotone and globally asymptotically stable (since changing sign to either of the variables turns the system Jacobian into a triangular Metzler matrix with negative diagonal entries) around its unique equilibrium.

We assume that y evolves on a much faster timescale than x (which is always feasible in practice, because the degradation of y may be tuned by design via catalytic degradation). Thus, once $x \geq \kappa_x$, y converges immediately to its *high* equilibrium $\bar{y} = \gamma/\delta$. To portray the actual behaviour of the biological system, we assume that the solution \bar{x} of $f(\bar{x}, \bar{y}) = b$ is a monotonically decreasing function of \bar{y} : it is larger when $\bar{y} = 0$ than when $\bar{y} = \gamma/\delta > 0$. Also, since the equilibrium concentration of a biological component depends on the ratio of its production and degradation (or dilution) rates, we assume that $f(x, y) = \beta(y)x$, where β is a positive increasing function, hence $\bar{x} = b/\beta(\bar{y})$. The simplified system becomes $\dot{x} = b - \beta_{\sigma(x)}x$, with $\beta_1 > \beta_0 > 0$ (where $\beta_0 = \beta_{\sigma(x)=0}$ etc.). Also the production rate b may depend on \bar{y} , as long as $\partial\bar{x}/\partial\bar{y} < 0$; for instance, we may have $\dot{x} = b_{\sigma(x)} - \beta x$, with $b_0 > b_1 > 0$ (where $b_0 = b_{\sigma(x)=0}$ etc.).

Set-reset motif. By interconnecting two reset modules we obtain the system in Fig. 1B, that automatically sets and re-sets its operation: each module, $i = 1, 2$, includes a recombinase X_i , which exclusively recognises its binding sites (purple triangles) and reorients the promoter to enable production of Y_i ; the binding sites are altered when the promoter is reoriented, so the recombinase can operate only if the promoter for the expression of Y_i is off (oriented in the opposite direction required for expression) and if the recombinase exceeds its threshold κ_{x1} . If recombinase X_1 exceeds κ_{x1} , then the promoter switches orientation to $p = p_1$. Similarly, if the promoter is oriented to the right, $p = p_1$, exclusively the recognition sites for X_2 are available; reorientation to $p = p_2$ occurs when X_2 exceeds κ_{x2} . The overall system can be described by the qualitative model:

$$\dot{x}_i = c_i - f_i(x_i, y_i), \quad \dot{y}_i = \gamma_i p_i(t) - \delta_i y_i, \quad (1)$$

where $p_1(t) = [1 - \sigma(t)]$ and $p_2(t) = \sigma(t)$, $c_1 = a > 0$ and $c_2 = b > 0$ are constant production rates, f_i are increasing

functions of both arguments, which are zero when the first argument is zero and tend to infinity when the first argument does (hence the existence of an equilibrium point is ensured), and $\gamma_i, \delta_i > 0$. Coupling between the two modules is due to function σ , which changes its value depending on its previous value and on when the state x_i exceeds its threshold κ_{xi} :

$$\sigma(t) = \begin{cases} 1 & \text{if } \begin{cases} \sigma(t^-) = 1, x_2(t) < \kappa_{x2}, \forall x_1(t) \\ \text{or} \\ \sigma(t^-) = 0, x_2(t) \geq \kappa_{x2}, \forall x_1(t) \end{cases} \\ 0 & \text{if } \begin{cases} \sigma(t^-) = 0, x_1(t) < \kappa_{x1}, \forall x_2(t) \\ \text{or} \\ \sigma(t^-) = 1, x_1(t) \geq \kappa_{x1}, \forall x_2(t) \end{cases} \end{cases} \quad (2)$$

Set $f_1(x_1, y_1) = \alpha(y_1)x_1$ and $f_2(x_2, y_2) = \beta(y_2)x_2$, with α and β positive increasing functions. When σ is kept constant, the overall system is monotone and globally asymptotically stable around its unique equilibrium: $[a/\alpha(\gamma_1/\delta_1), \gamma_1/\delta_1, b/\beta(0), 0]^\top$ when $\sigma \equiv 0$ and $[a/\alpha(0), 0, b/\beta(\gamma_2/\delta_2), \gamma_2/\delta_2]^\top$ when $\sigma \equiv 1$.

To study the behaviour under switching, we consider the simplified system obtained by assuming that y_i evolves on a much faster timescale than x_i : once $x_i \geq \kappa_{xi}$, y_i converges immediately to its *high* equilibrium $\bar{y}_i = \gamma_i/\delta_i$. Note that $\delta_1 \neq \delta_2$ in general. The simplified system becomes:

$$\dot{x}_1 = a - \alpha_\sigma x_1, \quad \dot{x}_2 = b - \beta_\sigma x_2, \quad (3)$$

with $a, b > 0$, $\alpha_0 > \alpha_1 > 0$ and $\beta_1 > \beta_0 > 0$.

Under the same timescale-separation assumptions, when the production rates depend on y_i , the simplified system is:

$$\dot{x}_1 = a_\sigma - \alpha x_1, \quad \dot{x}_2 = b_\sigma - \beta x_2, \quad (4)$$

with $\alpha, \beta > 0$, $a_1 > a_0 > 0$ and $b_0 > b_1 > 0$.

III. ANALYSIS OF THE SET-RESET MOTIF

We give *necessary and sufficient* conditions on the threshold values κ_{x1} and κ_{x2} to guarantee the existence of a periodic orbit for the simplified systems (3) and (4), providing analytic expressions for the corresponding period and amplitude.

Theorem 1: System (3), with $a, b > 0$, $\alpha_0 > \alpha_1 > 0$ and $\beta_1 > \beta_0 > 0$, under the switching rule (2), admits a non-constant periodic orbit if and only if

$$\frac{a}{\alpha_0} < \kappa_{x1} < \frac{a}{\alpha_1}, \quad \frac{b}{\beta_1} < \kappa_{x2} < \frac{b}{\beta_0}, \quad (5)$$

$$\Gamma(\kappa_{x1}, \kappa_{x2}) = h_1 \kappa_{x1} \kappa_{x2} + h_2 \kappa_{x1} + h_3 \kappa_{x2} > 0, \quad (6)$$

with $h_1 = \alpha_0 \beta_1 - \alpha_1 \beta_0$, $h_2 = b(\alpha_1 - \alpha_0)$, $h_3 = a(\beta_0 - \beta_1)$. The corresponding period is $T = T_1 + T_2$ and the amplitude is $\kappa_{x1} - q_1$ for x_1 and $\kappa_{x2} - q_2$ for x_2 , where T_1 and T_2 are the positive solutions of

$$T_2 = \psi_1(T_1) = \frac{1}{\alpha_1} \log \left[\frac{(\frac{a}{\alpha_1} - \frac{a}{\alpha_0}) + (\frac{a}{\alpha_0} - \kappa_{x1})e^{-\alpha_0 T_1}}{\frac{a}{\alpha_1} - \kappa_{x1}} \right], \quad (7)$$

$$T_1 = \psi_2(T_2) = \frac{1}{\beta_0} \log \left[\frac{(\frac{b}{\beta_0} - \frac{b}{\beta_1}) + (\frac{b}{\beta_1} - \kappa_{x2})e^{-\beta_1 T_2}}{\frac{b}{\beta_0} - \kappa_{x2}} \right], \quad (8)$$

while

$$q_1 = \kappa_{x1} e^{-\alpha_0 T_1} + (1 - e^{-\alpha_0 T_1})a/\alpha_0, \quad (9)$$

$$q_2 = \kappa_{x2} e^{-\beta_1 T_2} + (1 - e^{-\beta_1 T_2})b/\beta_1. \quad (10)$$

Proof: If the two thresholds do not take values between the *low* and the *high* equilibrium, then, in view of (2), the system converges to one of the two equilibria, depending on the initial conditions; hence, no periodic switching can occur. Therefore, (5) is necessary. Denote as $T_1(k)$ (respectively, $T_2(k)$) the time interval after which x_2 (resp. x_1) crosses its threshold for the k th time. The system trajectory starting from the initial conditions $x_1(0) = \kappa_{x_1}$ (known) and $x_2(0) = q_2$ (unknown) can be explicitly computed. Denoting $x_2(T_1) = \kappa_{x_2}$, $x_1(T_1) = q_1$ and $x_1(T_1 + T_2) = \kappa_{x_1}$ (with the index k for the T_i 's dropped for simplicity), a periodic orbit is achieved iff the following equations hold:

$$\kappa_{x_1} e^{-\alpha_0 T_1} + (1 - e^{-\alpha_0 T_1})a/\alpha_0 = q_1 \quad (11)$$

$$q_1 e^{-\alpha_1 T_2} + (1 - e^{-\alpha_1 T_2})a/\alpha_1 = \kappa_{x_1} \quad (12)$$

$$q_2 e^{-\beta_0 T_1} + (1 - e^{-\beta_0 T_1})b/\beta_0 = \kappa_{x_2} \quad (13)$$

$$\kappa_{x_2} e^{-\beta_1 T_2} + (1 - e^{-\beta_1 T_2})b/\beta_1 = q_2 \quad (14)$$

By substituting the expression of q_1 from (11) into (12) and the expression of q_2 from (14) into (13), after some algebraic manipulations we get $T_2 = \psi_1(T_1)$ as in (7) and $T_1 = \psi_2(T_2)$ as in (8). Hence, the sequence of time intervals $T_1(k)$ (resp. $T_2(k)$) evolves as $T_1(k+1) = \psi_2 \circ \psi_1(T_1(k)) \doteq \psi(T_1(k))$ (resp. $T_2(k+1) = \psi_1 \circ \psi_2(T_2(k))$). Under condition (5), for $i = 1, 2$, ψ_i is a strictly increasing, nonnegative and concave function, $\partial^2 \psi_i / \partial T_i^2 < 0$, $\psi_i(0) = 0$ and $\lim_{T_i \rightarrow \infty} \psi_i(T_i) = k_i > 0$. Hence, the two curves (qualitatively shown in Fig. 2A) have an intersection at the origin. They may also admit a nontrivial intersection, for $T_1, T_2 > 0$, which is then unique due to concavity. The nontrivial intersection exists if and only if $\psi'(0) = \partial \psi_1 / \partial T_1|_{T_1=0} \cdot \partial \psi_2 / \partial T_2|_{T_2=0} > 1$ (cf. [17, Theorem 2]), namely

$$\frac{\alpha_0 \kappa_{x_1} - a}{a - \alpha_1 \kappa_{x_1}} \cdot \frac{\beta_1 \kappa_{x_2} - b}{b - \beta_0 \kappa_{x_2}} > 1. \quad (15)$$

In fact, function $\psi = \psi_1 \circ \psi_2$ is nonnegative, strictly increasing and strictly concave: $\psi_1(\psi_2(\alpha T_a + \beta T_b)) \geq \psi_1(\alpha \psi_2(T_a) + \beta \psi_2(T_b)) \geq \alpha \psi_1(\psi_2(T_a)) + \beta \alpha \psi_1(\psi_2(T_b))$. Also, $\psi(0) = 0$. If $\psi'(0) > 1$, then the concave function $\phi(T_1) \doteq \psi(T_1) - T_1$ is positive in a right neighborhood of the origin and becomes negative after a certain value (since $\lim_{T_1 \rightarrow \infty} \phi'(T_1) = -1$), hence it admits a single positive root; conversely, if $\psi'(0) \leq 1$, then $\phi(T_1)$ is always negative for positive T_1 , hence there is no positive root. Therefore it must be $\psi'(0) > 1$, namely (15), which can be rewritten in the form $\Gamma(\kappa_{x_1}, \kappa_{x_2}) > 0$ as in (6).

Now, the sequence $T_1(k)$ satisfies $T_1(k+1) = \psi(T_1(k))$. Let \bar{T}_1 be the fixed point $\bar{T}_1 = \psi(\bar{T}_1)$. For $T_1(0) > 0$, we show that $T_1(k) \rightarrow \bar{T}_1$ asymptotically. In fact, due to the properties of ψ , if $T_1(k) > \bar{T}_1$, then $T_1(k) > \psi(T_1(k)) > \bar{T}_1$, hence the sequence decreases and it has a limit, which is necessarily the fixed point \bar{T}_1 . If instead $T_1(k) < \bar{T}_1$, then $T_1(k) < \psi(T_1(k)) < \bar{T}_1$, hence the sequence increases and it has a limit, the fixed point \bar{T}_1 . Hence, $T_1(k) \rightarrow \bar{T}_1$. Analogously, for $T_2(0) > 0$, $T_2(k) \rightarrow \bar{T}_2$.

The curve $\Gamma(\kappa_{x_1}, \kappa_{x_2}) = 0$ is a hyperbola with positive asymptotes $\kappa_{x_1} = \frac{a(\beta_1 - \beta_0)}{\alpha_0 \beta_1 - \alpha_1 \beta_0} < \frac{a}{\alpha_0}$ and $\kappa_{x_2} = \frac{b(\alpha_0 - \alpha_1)}{\alpha_0 \beta_1 - \alpha_1 \beta_0} < \frac{b}{\beta_1}$. Note that $\Gamma(\frac{a}{\alpha_0}, \frac{b}{\beta_1}) < 0$, while $\Gamma(0, 0) = \Gamma(\frac{a}{\alpha_0}, \frac{b}{\beta_0}) = \Gamma(\frac{a}{\alpha_1}, \frac{b}{\beta_1}) = 0$, and $\Gamma(\frac{a}{\alpha_1}, \frac{b}{\beta_0}) > 0$. Fig. 2B shows in blue the

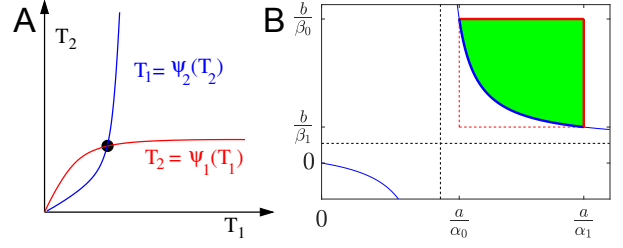


Fig. 2. A: **Determining the period.** The curves $T_2 = \psi_1(T_1)$ as in (7) and $T_1 = \psi_2(T_2)$ as in (8) in the (T_1, T_2) plane. A nontrivial intersection (with $T_1, T_2 > 0$) exists iff the product of the two first derivatives at the origin is larger than one. B: **Conditions for periodic behaviour.** In the $(\kappa_{x_1}, \kappa_{x_2})$ plane, the green set identifies the threshold choices that satisfy (5) and (6) and thus yield a periodic orbit for system (3) under the switching rule (2); the blue curve is the hyperbola $\Gamma(\kappa_{x_1}, \kappa_{x_2}) = 0$, the dashed black lines are its asymptotes, and the red lines are the sides of the rectangle in (5).

hyperbola $\Gamma(\kappa_{x_1}, \kappa_{x_2}) = 0$ and in green the set of $(\kappa_{x_1}, \kappa_{x_2})$ that satisfy both (5) and (6). As shown, choosing the thresholds in this set is necessary and sufficient for a periodic trajectory to exist, which then has period $T = \bar{T}_1 + \bar{T}_2$ and amplitude $\kappa_{x_1} - q_1$ for x_1 and $\kappa_{x_2} - q_2$ for x_2 . ■

Remark 1: If (5) and (6) are not satisfied, the system trajectories eventually chatter around (or converge to) an equilibrium depending on the initial conditions and the thresholds.

We now show positive invariance of the set

$$\mathcal{X} = \{0 \leq x_i \leq \kappa_{x_i}, i = 1, 2\} \quad (16)$$

and prove that convergence to the periodic orbit, whenever it exists, is guaranteed for all initial conditions in \mathcal{X} .

Proposition 1: If (5) holds, \mathcal{X} in (16) is a positively invariant set for system (3), with $a, b > 0$, $\alpha_0 > \alpha_1 > 0$ and $\beta_1 > \beta_0 > 0$, under the switching rule (2).

Proof: Invariance is guaranteed since $\dot{x}_i > 0$ when $x_i = 0$ and, in view of (5), $\dot{x}_i(t) < 0$ when $x_i(t^-) = \kappa_{x_i}$. Indeed, if $x_1(t^-) = \kappa_{x_1}$, $\sigma(t) = 0$, hence $\dot{x}_1(t) < a - \alpha_0 \kappa_{x_1} < 0$; if $x_2(t^-) = \kappa_{x_2}$, $\sigma(t) = 1$, hence $\dot{x}_2(t) < b - \beta_1 \kappa_{x_2} < 0$. ■

Theorem 2: If (5) and (6) hold, the trajectories of system (3), with $a, b > 0$, $\alpha_0 > \alpha_1 > 0$ and $\beta_1 > \beta_0 > 0$, under the switching rule (2), converge to a periodic orbit for all initial conditions in the set \mathcal{X} in (16).

Proof: We can build a Poincaré map as follows (see also Fig. 3A): for $k = 0, 1, 2, \dots$, we take a switching point with $x_1 = x_1(k)$ and $x_2 = \kappa_{x_2}$ (the red point in Fig. 3A). Starting from this point, at time $T_1(k)$ we reach a new switching point with $x_1 = \kappa_{x_1}$ and $x_2 = x_2(T_1(k))$ (the magenta point in Fig. 3A). From there, $T_2(k)$ time units after switching, we reach a new switching point with coordinates $x_1 = x_1(k+1) = x_1(T_1(k) + T_2(k))$ and $x_2 = \kappa_{x_2}$ (the cyan point in Fig. 3A), which lies again on the line $x_2 = \kappa_{x_2}$. The Poincaré map from $x_1(k)$ to $x_1(k+1)$, both corresponding to $x_2 = \kappa_{x_2}$, can be written by adopting the same expressions as in the proof of Theorem 1 and turns out to be the time-varying map:

$$x_1(k+1) = A(k)x_1(k) + C(k), \quad (17)$$

where $A(k) = e^{-\alpha_0 T_1(k)} e^{-\alpha_1 T_2(k)}$ and $C(k) = (1 - e^{-\alpha_0 T_1(k)})e^{-\alpha_1 T_2(k)}a/\alpha_0 + (1 - e^{-\alpha_1 T_2(k)})a/\alpha_1$. As shown in the proof of Theorem 1, asymptotically $T_1(k), T_2(k) \rightarrow \bar{T}_1, \bar{T}_2$, hence $A(k) \rightarrow \bar{A}$ and $C(k) \rightarrow \bar{C}$. Then (17) converges

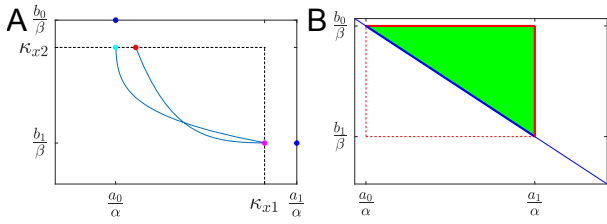


Fig. 3. A: Iterations of the Poincaré map in the (x_1, x_2) plane; the dashed black lines mark the threshold values, the two blue dots are the equilibrium values for $\sigma = 0$ and for $\sigma = 1$. Starting from the red dot with $x_2 = \kappa_{x_2}$, the system trajectory reaches the magenta dot and then, after switching, reaches the cyan dot that is again on the line $x_2 = \kappa_{x_2}$. B: In the $(\kappa_{x_1}, \kappa_{x_2})$ plane, the green set identifies the threshold choices that satisfy (18) and (19), yielding a periodic orbit for (4) under the switching rule (2); the blue line is $\Lambda(\kappa_{x_1}, \kappa_{x_2}) = 0$, and the red lines are the sides of the rectangle in (18).

to the time-invariant map $x_1(k+1) = \bar{A}x_1(k) + \bar{C}$ and, since $\bar{A} = e^{-\alpha_0 T_1} e^{-\alpha_1 T_2} < 1$, the fixed point of this discrete-time system is asymptotically stable, globally within \mathcal{X} (due to the converging-input converging-state property [18] of stable linear systems). Therefore, asymptotic convergence to the periodic orbit of the continuous-time system is guaranteed for all initial conditions in \mathcal{X} . ■

For system (4), analogous results can be proven.

Theorem 3: System (4), with $\alpha, \beta > 0$, $a_1 > a_0 > 0$ and $b_0 > b_1 > 0$, under the switching rule (2), admits a non-constant periodic orbit if and only if

$$\frac{a_0}{\alpha} < \kappa_{x_1} < \frac{a_1}{\alpha}, \quad \frac{b_1}{\beta} < \kappa_{x_2} < \frac{b_0}{\beta}, \quad (18)$$

$$\Lambda(\kappa_{x_1}, \kappa_{x_2}) = m_1 \kappa_{x_1} + m_2 \kappa_{x_2} + m_3 > 0, \quad (19)$$

with $m_1 = \alpha(b_0 - b_1)$, $h_2 = \beta(a_1 - a_0)$, and $m_3 = a_0 b_1 - a_1 b_0$. The corresponding period is $T = T_1 + T_2$ and the amplitude is $\kappa_{x_1} - q_1$ for x_1 and $\kappa_{x_2} - q_2$ for x_2 , where T_1 and T_2 are the positive solutions of

$$T_2 = \psi_1(T_1) = \frac{1}{\alpha} \log \left[\frac{(\frac{a_1}{\alpha} - \frac{a_0}{\alpha}) + (\frac{a_0}{\alpha} - \kappa_{x_1}) e^{-\alpha T_1}}{\frac{a_1}{\alpha} - \kappa_{x_1}} \right], \quad (20)$$

$$T_1 = \psi_2(T_2) = \frac{1}{\beta} \log \left[\frac{(\frac{b_0}{\beta} - \frac{b_1}{\beta}) + (\frac{b_1}{\beta} - \kappa_{x_2}) e^{-\beta T_2}}{\frac{b_0}{\beta} - \kappa_{x_2}} \right], \quad (21)$$

and

$$q_1 = \kappa_{x_1} e^{-\alpha T_1} + (1 - e^{-\alpha T_1}) a_0 / \alpha, \quad (22)$$

$$q_2 = \kappa_{x_2} e^{-\beta T_2} + (1 - e^{-\beta T_2}) b_1 / \beta. \quad (23)$$

Proof: We can proceed as in the proof of Theorem 1. We get $T_2 = \psi_1(T_1)$ as in (20) and $T_1 = \psi_2(T_2)$ as in (21); under condition (18), for $i = 1, 2$, ψ_i is an increasing, positive concave function, $\partial^2 \psi_i / \partial T_i^2 < 0$, $\psi_i(0) = 0$ and $\lim_{T_i \rightarrow \infty} \psi_i(T_i) = k_i > 0$. Therefore, the two curves have an intersection at the origin (cf. Fig. 2A). They may also have a nontrivial intersection, for $T_1, T_2 > 0$, which is then unique due to concavity and exists if and only if $\partial \psi_1 / \partial T_1|_{T_1=0} \cdot \partial \psi_2 / \partial T_2|_{T_2=0} > 1$ (cf. [17, Theorem 2]), i.e.

$$\frac{\alpha \kappa_{x_1} - a_0}{a_1 - \alpha \kappa_{x_1}} \cdot \frac{\beta \kappa_{x_2} - b_1}{b_0 - \beta \kappa_{x_2}} > 1,$$

which can be rewritten in the form $\Lambda(\kappa_{x_1}, \kappa_{x_2}) > 0$ as in (19). $\Lambda(\kappa_{x_1}, \kappa_{x_2}) = 0$ is a line; $\Lambda(\frac{a_0}{\alpha}, \frac{b_1}{\beta}) < 0$, while $\Lambda(\frac{a_0}{\alpha}, \frac{b_0}{\beta}) = \Lambda(\frac{a_1}{\alpha}, \frac{b_1}{\beta}) = 0$, and $\Lambda(\frac{a_1}{\alpha}, \frac{b_0}{\beta}) > 0$. Fig. 3B shows in blue the

line $\Lambda(\kappa_{x_1}, \kappa_{x_2}) = 0$ and in green the set of $(\kappa_{x_1}, \kappa_{x_2})$ that satisfy both (18) and (19). ■

The next results can also be proven along the same lines as Proposition 1 and Theorem 2.

Proposition 2: If (18) holds, \mathcal{X} in (16) is a positively invariant set for system (4), with $\alpha, \beta > 0$, $a_1 > a_0 > 0$ and $b_0 > b_1 > 0$, under the switching rule (2).

Theorem 4: If (18) and (19) hold, the trajectories of system (4), with $\alpha, \beta > 0$, $a_1 > a_0 > 0$ and $b_0 > b_1 > 0$, under the switching rule (2), converge to a periodic orbit for all initial conditions in the set \mathcal{X} in (16).

IV. REALISATIONS OF THE SET-RESET MOTIF

A recombinase-protease (RP) implementation. Our first realisation, illustrated in Fig. 4A, consists of two pairs of recombinases X_1 and X_2 [1] and two proteases Y_1 and Y_2 [19]; the protease Y_i promotes degradation of the recombinase X_i . When the promoter is oriented to the right, $p = p_1$, it expresses Y_1 with reaction rate constant γ ; when the promoter is oriented to the left, $p = p_2$, it produces Y_2 at the same rate γ . Because viral proteases exhibit strong specificity for short target sites, the protease Y_i can be designed to target and degrade exclusively the recombinase X_i , $i = 1, 2$ [19]. The degradation rate for both proteases is δ . The recombinases X_1 and X_2 are respectively produced at rates θ_1 and θ_2 , and both decay at rate ϕ . The recombinases X_i , $i = 1, 2$ cause a switch in the promoter orientation only when they exceed their thresholds κ_{x_i} and their recognition sites are available. We assume that the promoter orientation is a variable that switches deterministically between two values depending on the concentration of the recombinases X_1 and X_2 relative to their thresholds κ_{x_1} and κ_{x_2} , and that species X_1 , X_2 , Y_1 and Y_2 exist at high-copy numbers. Hence, their interactions (Fig. 4A) can be modelled by the macroscopic chemical reactions: $\emptyset \xrightarrow{\gamma p_i} Y_i$ (recombinase-regulated production), $\emptyset \xrightarrow{\theta_i} X_i$ (constitutive production), $Y_i \xrightarrow{\delta} \emptyset$ and $X_i \xrightarrow{\phi} \emptyset$ (constitutive degradation), $X_i \xrightarrow{\rho g_i} \emptyset$ (protease-catalysed degradation), occurring in Module $i = 1, 2$. We assume protease-catalysed degradation is Michaelian, with $g_i = \frac{y_i}{y_i + \kappa_{y_i}}$, $i = 1, 2$. At any given time the promoter can be oriented *exclusively* to the right ($p_1 = 1$ and $p_2 = 0$) or to the left ($p_1 = 0$ and $p_2 = 1$). Therefore $p_1 = (1 - \sigma)$ and $p_2 = \sigma$, with switching variable $\sigma = \{0, 1\}$. The current value of σ depends on its previous value as well as on the concentration of the recombinases X_1 and X_2 relative to κ_{x_1} and κ_{x_2} , as in (2). The model of the RP circuit, derived from the reactions using the law of mass action, is:

$$\dot{x}_i = \theta_i - \phi x_i - \rho g_i(y_i) x_i, \quad \dot{y}_i = \gamma p_i - \delta y_i, \quad i = 1, 2,$$

where the two modules operate together, coupled exclusively by the orientation of the promoter. The RP system falls into the class (1). With either promoter orientation, the protease and recombinase concentrations in each module converge exponentially to a globally asymptotically stable equilibrium: when $\sigma = 0$, $\bar{x}_1 = \theta_1 / \phi$, $\bar{y}_1 = 0$, $\bar{x}_2 = \theta_2 / [\phi + \rho \frac{\gamma / \delta}{\gamma / \delta + \kappa_{y_2}}]$, $\bar{y}_2 = \gamma / \delta$; when $\sigma = 1$, $\bar{x}_1 = \theta_1 / [\phi + \rho \frac{\gamma / \delta}{\gamma / \delta + \kappa_{y_1}}]$, $\bar{y}_1 = \gamma / \delta$, $\bar{x}_2 = \theta_2 / \phi$, $\bar{y}_2 = 0$.

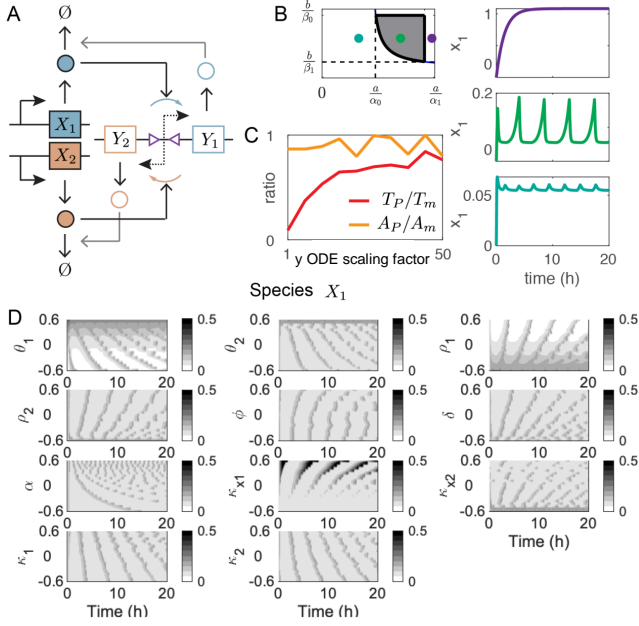


Fig. 4. Recombinase-protease (RP) realisation of the set-reset circuit A: The circuit combines two recombinase and protease pairs: the recombinase induces re-orientation of the promoter controlling expression of the protease, which in turn catalyses recombinase degradation. **B:** Top left: sketch of the region in the threshold plane that enables a periodic behaviour; right column: example solutions of the circuit, corresponding to the three threshold choices highlighted in the same color in the threshold plane, with initial conditions $(0, 0)$ and parameters as in Table I. The green choice yields a regular periodic behaviour, as expected (Theorems 1 and 2). The violet and cyan choices correspond to thresholds out of the prescribed region and, as expected, instead of a periodic behaviour we see monotonic convergence, violet, and chattering, cyan (cf. Remark 1). **C:** Ratio of predicted and simulated period and amplitude (T_p/T_m , and A_p/A_m), plotted against a nondimensional factor scaling the dynamics of y_i ; predictions use the expressions in Theorem 1 for the 2-dimensional system, while the complete 4-dimensional system is simulated. The larger the scaling factor, the faster y_i converges to steady state, and the closer the simulated period is to the theoretical prediction. **D:** Sensitivity analysis; the color intensity represents the concentration of x_1 at each time point on the x-axis, mapped to the scale on the right of each sub-figure. A single parameter is varied in each plot (y-axis is in logarithmic scale), while others are held fixed and equal to their nominal value listed in Table I.

If y_i quickly reach their steady state, we can approximate the system as in (3), with $a = \theta_1$, $b = \theta_2$, $\alpha_1 = \beta_0 = \phi$, $\alpha_0 = \phi + \rho \frac{\gamma/\delta}{\gamma/\delta + \kappa_{y1}}$ and $\beta_1 = \phi + \rho \frac{\gamma/\delta}{\gamma/\delta + \kappa_{y2}}$. Hence, Theorems 1 and 2 in Section III hold: convergence to a periodic behaviour for all initial conditions in \mathcal{X} in (16) occurs if and only if the thresholds values κ_{x1} and κ_{x2} satisfy (5) and (6).

A recombinase-repressor (RR) implementation. The second realisation of the set-reset system is schematically illustrated in Fig. 5A: expression of the recombinases X_1 and X_2 is now regulated by repressors Y_1 and Y_2 , hence we call this a recombinase-repressor (RR) implementation. The remaining elements of the circuit operate identically to the RP realisation.

The RR chemical reactions are: $\emptyset \xrightarrow{\gamma p_i} Y_i$ (recombinase-regulated production), $\emptyset \xrightarrow{\theta_i g_i} X_i$ (repressor-regulated production), $Y_i \xrightarrow{\delta} \emptyset$ and $X_i \xrightarrow{\phi} \emptyset$ (constitutive degradation), with $g_i = \frac{\kappa_{y_i}}{y_i + \kappa_{y_i}}$, $i = 1, 2$. Defining the switching variable σ and the thresholds as in the previous section, the corresponding dynamics can be derived using the law of mass action:

$$\dot{x}_i = \theta_i g_i(y_i) - \phi x_i, \quad \dot{y}_i = \gamma p_i - \delta y_i, \quad i = 1, 2,$$

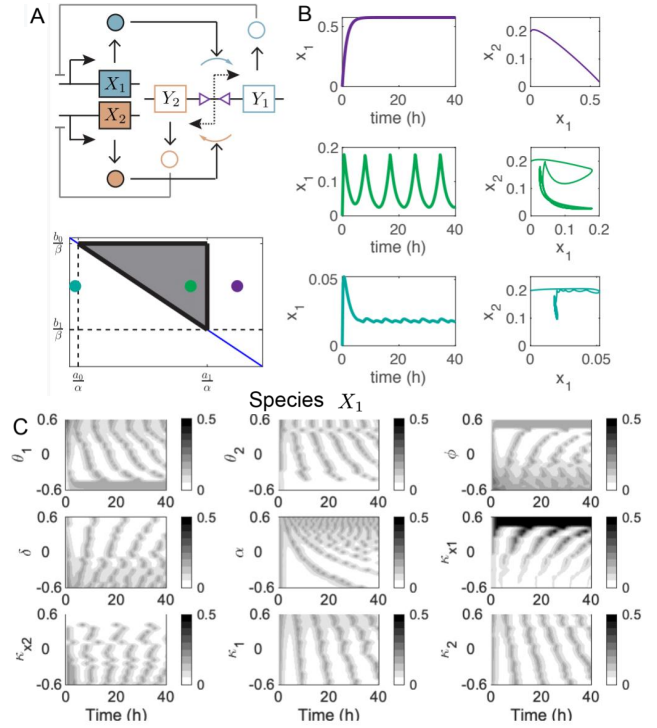


Fig. 5. Recombinase-repressor (RR) realisation of the set-reset circuit. A: The circuit combines two recombinase and repressor pairs: the recombinase induces re-orientation of the promoter controlling expression of the repressors. **Bottom:** sketch of the region in the threshold plane that enables a periodic behaviour. **B:** Example solutions of the circuit (in time and in phase space) corresponding to the three threshold choices highlighted at the bottom of panel A, with initial conditions $(0, 200nM)$ and parameters as in Table I. The green choice corresponds to thresholds within the gray region and yields a regular periodic behaviour, as expected (Theorems 3 and 4). The violet and cyan choices correspond to thresholds out of the gray region and, as expected, instead of a periodic behaviour we see monotonic convergence, violet, and chattering, cyan (cf. Remark 1). **C:** Sensitivity analysis; the color intensity represents the concentration of x_1 at each time point on the x-axis, mapped to the scale on the right of each sub-figure. A single parameter is varied in each plot (y-axis is in logarithmic scale), while others are held fixed and equal to their nominal value listed in Table I.

where $p_1 = 1 - \sigma$ and $p_2 = \sigma$. Under time-scale separation assumptions, the approximated system has the form (4), with $a_0 = \theta_1 \frac{\kappa_{y1}}{\gamma/\delta + \kappa_{y1}}$, $a_1 = \theta_1$, $b_0 = \theta_2$, $b_1 = \theta_2 \frac{\kappa_{y2}}{\gamma/\delta + \kappa_{y2}}$, $\alpha = \beta = \phi$. Hence, Theorems 3 and 4 in Section III hold: to converge to a periodic behaviour for all initial conditions in \mathcal{X} in (16) it is necessary and sufficient to pick the thresholds κ_{x1} and κ_{x2} so that (18) and (19) are satisfied.

Numerical simulations. We used MATLAB to integrate the ODE models for the RP and RR implementations, using the nominal parameters listed in Table I (unless otherwise noted). Example trajectories (Fig. 4B and Fig. 5B) show that periodic switching occurs only when the parameters are within the regions computed from our theoretical predictions. When using distinct degradation rates (e.g., $\delta_1 \neq \delta_2$), oscillations still occur but symmetry within the modules is lost (not shown). For the RP circuit, we verify in Fig. 4C that, as the steady-state convergence of y_i becomes faster, the period and amplitude in simulated oscillations (4-dimensional system) converge to the analytical predictions obtained in Theorem 1 under time-scale separation assumptions (2-dimensional system). We note that the RP oscillatory region in the plane $(\kappa_{x1}, \kappa_{x2})$ is larger than

the oscillatory region of the RR implementation, indicating that the RP realisation may be more robust.

In Fig. 4D and Fig. 5C we report a sensitivity analysis of the models, in which each parameter varies from one fourth to four times its nominal value (reported in Table I). The sensitivity analysis shows that production rate θ_i , degradation rate ϕ and threshold κ_i are the key for periodic behaviour. Indeed, increasing θ_i increases the lower bound required for κ_{xi} , which then becomes larger than κ_{xi} ; while decreasing θ_i prevents X_i from reaching its threshold κ_{xi} . The range of parameters explored in the sensitivity plots in Fig. 4D and Fig. 5C do not show a lower bound for θ_i and an upper bound for κ_{xi} (resp. an upper bound for θ_i and a lower bound for κ_{xi}) because the extreme parameter values we picked were still within the gray area; however, we have explored a larger parameter range, not shown here, and we have observed the bounds as predicted. Overall, the simulation results agree with the necessary and sufficient conditions for the existence of periodic behaviours derived in Section III. Also, the faster the dynamics of y_i , the closer the period and amplitude of x_i are to those computed based on the exact analytic expressions obtained under time-scale separation assumptions (Fig. 4C). Both implementations perform as expected in numerical simulation, although the sensitivity analysis suggests that RP may be more robust. In practice, the implementation choice will depend on availability of parts; neither the protease nor the repressor are required to be highly cooperative, but their Michaelis constants (thresholds) should satisfy the requirements outlined here.

TABLE I
SIMULATION PARAMETERS FOR THE RP AND RR CIRCUITS

Parameter	Circuit	Value	Other studies
θ_1, θ_2 (M/s)	RP	$2.08 \cdot 10^{-10}$	$2.8 \cdot 10^{-11} - 2.8 \cdot 10^{-8}$
γ (M/s)	RP	$5.2 \cdot 10^{-10}$	[20], [21]
θ_1, θ_2 (M/s)	RR	$1.11 \cdot 10^{-10}$	$2.8 \cdot 10^{-11} - 2.8 \cdot 10^{-8}$
γ (M/s)	RR	$2.22 \cdot 10^{-10}$	[20], [21]
ϕ, δ (/s)	RP/RR	$1.93 \cdot 10^{-4}, \delta = 4\phi$	$10^{-4} - 10^{-3}$
ρ (/s)	RP	$3.85 \cdot 10^{-3}$	[22]
κ_{x1}, κ_{x2} (nM)	RP/RR	200	
κ_{y1}, κ_{y2} (nM)	RP/RR	100	

V. CONCLUSIONS AND OUTLOOK

We proposed a general recombinase-based motif to achieve periodic switching, along with necessary and sufficient conditions that relate switching thresholds with the emergence of periodic behaviours. Two realisations, shown to exhibit periodic switching in a realistic parameter range, suggest viability of an experimental implementation. Our numerical sensitivity analysis indicates that a desired period may be achieved by tuning parameters such as protein production and degradation (e.g., by strengthening promoter regions and using degradation tags). Both realisations could be classified as relaxation oscillators, which are generally more robust than phase oscillators [8], [9], [16], [23]. Preliminary results indicate that oscillations can be achieved with positive-feedback variants of the networks considered here (for example, X_i switches expression from Y_i to Y_j , while Y_i activates X_i , $i = 1, 2, j = 2, 1$).

Our deterministic models assume deterministic promoter switching as the recombinase concentration exceeds a given

threshold. This is a reasonable representation of a system operating at high copy number in a cell-free, *in vitro* testbed. A recombinase circuit *in vivo* would be better represented as a stochastic hybrid system, since only one copy of each promoter would be present in the system, and its reorientation would be a stochastic event. Future work is aimed at providing a formal analysis of the stochastic operation of this motif.

REFERENCES

- [1] C. A. Merrick, J. Zhao, and S. J. Rosser, "Serine integrases: advancing synthetic biology," *ACS Syn. Biol.*, vol. 7, no. 2, pp. 299–310, 2018.
- [2] J. Bonnet, P. Subsoontorn, and D. Endy, "Rewritable digital data storage in live cells via engineered control of recombination directionality," *Proc. Natl. Acad. Sci. USA*, vol. 109, no. 23, pp. 8884–8889, 2012.
- [3] N. Roquet, A. P. Soleimany, A. C. Ferris, S. Aaronson, and T. K. Lu, "Synthetic recombinase-based state machines in living cells," *Science*, vol. 353, p. 6297, p. aad8559, 2016.
- [4] B. H. Weinberg, N. H. Pham, L. D. Caraballo, T. Lozanoski, A. Engel, S. Bhatia, and W. W. Wong, "Large-scale design of robust genetic circuits with multiple inputs and outputs for mammalian cells," *Nature biotech.*, vol. 35, no. 5, p. 453, 2017.
- [5] T. Follard, H. Steel, T. P. Prescott, G. Wadhams, L. J. Rothschild, and A. Papachristodoulou, "A synthetic recombinase-based feedback loop results in robust expression," *ACS Syn. Biol.*, vol. 6, no. 9, pp. 1663–1671, 2017.
- [6] T. F. Schubert Jr. and E. M. Kim, *Fundamentals of Electronics: Book 4 – Oscillators and Advanced Electronics Topics*, Morgan & Claypool Publishers, 2016.
- [7] B. Novák, and J. Tyson, "Design principles of biochemical oscillators" *Nat. Rev. Mol. Cell Biol.*, vol. 9, no. 12, pp. 981, 2008.
- [8] T. Y. C. Tsai, Y. S. Choi, W. Ma, J. R. Pomerening, C. Tang, and J. E. Ferrell, "Robust, tunable biological oscillations from interlinked positive and negative feedback loops." *Science*, vol. 321, no. 5885, pp.126–129, 2008.
- [9] D. McMillen, N. Kopell, J. Hasty, and J. J. Collins, "Synchronizing genetic relaxation oscillators by intercell signaling." *Proc. Natl. Acad. Sci. USA*, vol. 99, no. 2, pp 679–684, 2002.
- [10] D. Liberzon, *Switching in Systems and Control*, ser. Systems and Control: Foundations and Applications. Birkhäuser, Boston, 2003.
- [11] R. Goebel, R. G. Sanfelice, and A. R. Teel, *Hybrid Dynamical Systems: Modeling, Stability, and Robustness*. Princeton University Press, 2012.
- [12] F. Blanchini, P. Colaneri, and M. E. Valcher, "Switched positive linear systems," *Foundations and Trends in Systems and Control*, vol. 2, no. 2, pp. 101–273, 2015.
- [13] S. Jayanthi and D. Del Vecchio, "Retractivity attenuation in biomolecular systems based on timescale separation", *IEEE Transactions on Automatic Control*, vol. 56, no. 4, pp. 748–761, 2001.
- [14] H. K. Khalil, *Nonlinear systems (3rd Ed.)*. Prentice-Hall, 2002.
- [15] P. Kokotović, H. K. Khalil, and J. O'Reilly, *Singular Perturbation Methods in Control: Analysis and Design*. SIAM, Philadelphia (PA), USA, 1999.
- [16] C. Kut, V. Golkhou, and J. S. Bader, "Analytical approximations for the amplitude and period of a relaxation oscillator", *BMC Syst. Biol.*, vol. 3, no. 1, p. 6, 2009.
- [17] G. Giordano and F. Blanchini, "Flow-inducing networks", *IEEE Control Systems Letters*, vol. 1, no. 1, pp. 44–49, 2017.
- [18] E. D. Sontag, "A remark on the converging-input converging-state property", *IEEE Trans. Autom. Control*, vol. 48, no. 2, pp. 313–314, 2003.
- [19] X. J. Gao, L. S. Chong, M. S. Kim, and M. B. Elowitz, "Programmable protein circuits in living cells," *Science*, vol. 361, no. 6408, pp. 1252–1258, 2018.
- [20] Y. Qian, H.-H. Huang, J. I. Jiménez, and D. Del Vecchio, "Resource competition shapes the response of genetic circuits," *ACS Syn. Biol.*, vol. 6, no. 7, pp. 1263–1272, 2017.
- [21] S. Basu, Y. Gerchman, C. H. Collins, F. H. Arnold, and R. Weiss, "A synthetic multicellular system for programmed pattern formation," *Nature*, vol. 434, no. 7037, pp. 1130–1134, 2005.
- [22] J. Kim, I. Khetarpal, S. Sen, and R. M. Murray, "Synthetic circuit for exact adaptation and fold-change detection," *Nucleic acids res.*, vol. 42, no. 9, pp. 6078–6089, 2014.
- [23] C. Cuba Samaniego, G. Giordano, and E. Franco, "Design and analysis of a biomolecular positive-feedback oscillator", *Proc. IEEE Conference on Decision and Control*, 2018, pp. 1083–1088.